NANO LETTERS

Letter

pubs.acs.org/NanoLett

Ultrafast Polarization Response of an Optically Trapped Single Ferroelectric Nanowire

Sanghee Nah,[†,‡,⊥] Yi-Hong Kuo,[§,⊥] Frank Chen,[§] Joonsuk Park,[†] Robert Sinclair,[†] and Aaron M. Lindenberg[†,‡,∥,*]

[†]Department of Materials Science and Engineering, Stanford University, Stanford, California 94305, United States

[‡]Stanford Institute for Materials and Energy Sciences, SLAC National Accelerator Laboratory, 2575 Sand Hill Road, Menlo Park, California 94025, United States

[§]Department of Electrical Engineering, Stanford University, Stanford, California 94305, United States

[∥]Stanford PULSE Institute, SLAC National Accelerator Laboratory, Menlo Park, California 94025, United States

Supporting Information

ABSTRACT: One-dimensional potassium niobate nanowires are of interest as building blocks in integrated piezoelectric devices, exhibiting large nonlinear optical and piezoelectric responses. Here we present femtosecond measurements of light-induced polarization dynamics within an optically trapped ferroelectric nanowire, using the second-order nonlinear susceptibility as a real-time structural probe. Large amplitude, reversible modulations of the nonlinear susceptibility are observed within single nanowires at megahertz repetition rates, developing on few-picosecond time-scales, associated with anomalous coupling of light into the nanowire.

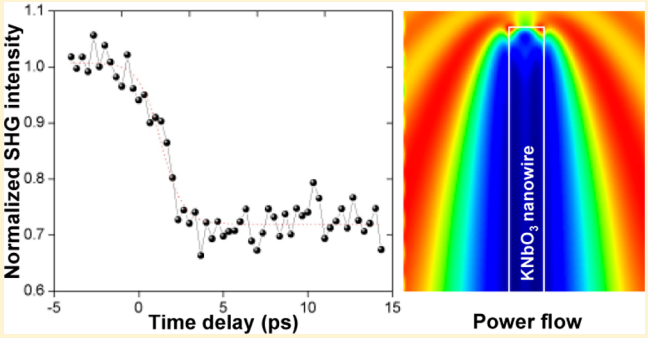

Ferroelectric potassium niobate ($KNbO_3$) exhibits large refractive indices and high effective nonlinear optical and piezoelectric coefficients,[1−4] which have led to its development in lead-free piezoelectric nanodevices and nanogenerators.[5,6] More recently, enhanced piezoelectricity from a low-symmetry monoclinic phase has been discovered and attracted significant interest to alkali niobate nanostructures.[7−9] The coupling of light to nanoscale ferroelectrics enables novel means of engineering and manipulating their coupled degrees of freedom and inducing new functionality, including photoferroelectric effects and other opto-mechanical responses.[10−16] Because one-dimensional nanowires with subwavelength diameters exhibit modified light-matter interactions such as field enhancements, light-confinement, waveguiding, and enhanced nonlinear optical responses,[9,17−19] they represent a previously unexplored means of coupling to the ferroelectric, piezoelectric, and structural phase transitions exhibited by $KNbO_3$ and related materials and novel opportunities for dynamic tuning of these properties in addition to subwavelength microscopy.[1,5,7,20−24] Here, we present time-resolved measurements of the dynamics of individual $KNbO_3$ nanowires using transient nonlinear optical microscopy integrated into an optical trapping apparatus. These measurements capture for the first time the femtosecond time scale structural dynamics occurring within a single free-standing ferroelectric nanowire inside an optical trap and can be explained by anomalous coupling of light into the nanowire, associated with an enhanced absorption cross-section by the nanowire embedded within the light field of the pump pulse.[17,25−33]

Optical trapping enables manipulation of single nanostructures in three dimensions and characterization of their optical properties.[34−36] Nanowires with high aspect ratios tend to be aligned along the optical axis of the trapping beam in the trap.[37,38] Nonlinear second harmonic generation (SHG) techniques allow one to probe the structural symmetry of the nanowire and associated carrier relaxation dynamics[32,39] as encoded in the second-order nonlinear optical susceptibility ($\chi^{(2)}$), sensitive to the deviation from centrosymmetry within the crystallographic unit cell, without being influenced by substrate effects.[40−42] Upon photoexcitation, incident photons are coupled into one end of a nanowire and waveguided along the nanowire length, with the fundamental generating the second harmonic along the length of the nanowire.[1]

One-dimensional single-crystalline $KNbO_3$ nanowires were synthesized by a hydrothermal method at low temperature.[9] In a typical reaction, 15 g of potassium hydroxide (Sigma-Aldrich) is dissolved in deionized water (15 mL) making an alkaline aqueous solution. After sonicating for 20 min, 0.84 g of niobium metal powder (Alfa Aesar) was added to the solution as a niobium ion source. The solution was transferred to a Teflon-lined autoclave and kept in an oven at 150 °C for 12 h.

Received: March 25, 2014
Revised: June 24, 2014
Published: July 22, 2014

After cooling the autoclave to room temperature, the solution was diluted with deionized water and purified by repeated centrifuging to remove the supernatant and collect the nanowire precipitate until the pH became 7. The precipitate was dried in an oven at 80 °C for 10 h.

To characterize the nanowires, transmission electron microscope (TEM) and selected area electron diffraction (SAED) images were taken using a FEI Titan 80−300 environmental TEM operating at 80 kV. The synthesized nanowires were ∼100 nm in diameter and 2−3 μm in length as shown in Figure 1a. The high-resolution TEM image in Figure 1b confirms the pseudocubic lattice parameters in the orthorhombic phase along the orthorhombic [100] and [011] axes with lattice spacings consistent with literature values.[43] The growth axis of the nanowire is parallel to the [011] direction and the spontaneous polarization is along the [001] direction (c-axis), which is 45° off the long axis of the nanowire. The SAED pattern (inset) using a 100 nm-size aperture confirms that the nanowire is single crystalline and orthorhombic.

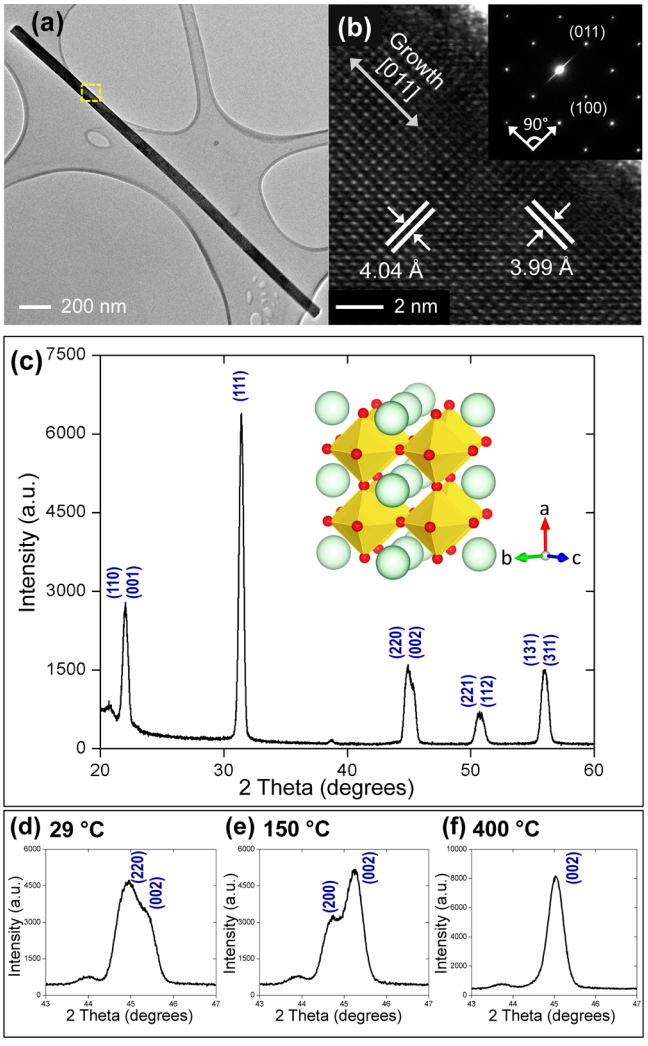

Figure 1. (a) TEM image of a single nanowire with a diameter of 67 nm and a length of 2.58 μm. (b) High-resolution TEM image from the selected area (yellow) in part a with indicated pseudocubic lattice parameters and growth axis. The SAED pattern (inset) indicates that the nanowire is single crystalline and orthorhombic. (c) XRD pattern of the nanowire power at room temperature. Selected-range XRD patterns of (d) orthorhombic phase at room temperature, (e) tetragonal phase at 150 °C, and (f) cubic phase at 400 °C.

We measure X-ray diffraction (XRD) patterns of the $KNbO_3$ nanowire powder using an X-ray diffractometer (X'Pert 2, PANalytical) with Cu Kα radiation as shown in Figure 1c. The XRD pattern was measured in the Bragg−Brentano geometry for the nanowires deposited on a silicon wafer. As a function of temperature, we observe the well-known orthorhombic-tetragonal and tetragonal-cubic transitions. Figure 1d shows two Bragg XRD peaks corresponding to the (220) and (002) orthorhombic phase reflections at room temperature. As temperature was increased, we observed the (200) and (002) tetragonal peaks at temperature 150 °C (Figure 1e), and the (002) cubic phase at 400 °C (Figure 1f). As shown in Figure 1e, the phase transition from orthorhombic to tetragonal took place at a lower temperature than the reported bulk transition temperature, 200 °C, consistent with prior measurements.[44−46] The TEM images and XRD patterns confirm that the synthesis performed using a Teflon-lined autoclave (125 mL) produced orthorhombic nanowires instead of monoclinic structures[9] due to the low pressure built up inside the autoclave during the growth reaction.[47]

To examine individual nanowires using an optical trapping setup, an aqueous sample chamber was prepared using two coverslips. A small amount of dried nanowires (0.001 g) was dispersed in deionized water (3 mL) and 2 μL of the solution was placed on a 130 μm-thick glass coverslip. The working distance of the oil-immersion objective, 200 μm, limited the thickness of the glass coverslip. A 250 μm-thick quartz coverslip was placed on top of the glass coverslip with two layers of Scotch tape creating a 260 μm-spacing to confine the solution.

Figure 2a shows a schematic diagram of the experimental setup using a Ti:sapphire pulsed laser (Femtolasers XL 500, 75 fs pulse duration, 5.12 MHz repetition rate, 800 nm). One portion of the beam was used as a probe beam and the other portion was used to produce a 4.66 eV (bulk bandgap[43] = 3.19 eV) pump beam at the third harmonic, by passing through two BBO crystals (β-barium borate). As an optical trapping beam, a 532 nm CW laser was expanded to overfill the back aperture of a high numerical aperture (NA) objective (oil-immersion 100×, NA 1.3). The probe beam (at 800 nm, below bandgap) and the trapping beam were focused on a single nanowire in an aqueous chamber placed on a piezoelectric sample stage through the high NA objective. A UV objective was placed to focus the pump beam onto the same nanowire and collect the reradiated SHG signals as a condenser. The incident fluences for the pump beam and the probe beam at the nanowire were 1 mJ/cm^2 and 0.1 J/cm^2, respectively. Independent measurements of the instrument temporal resolution indicate an upper bound of 400 fs. We employed a photomultiplier tube (PMT) to detect SHG photons and a photon counter to record the number of SHG photons as a function of time delay between pump and probe. Optical images were recorded using an electron multiplying charge coupled device (EMCCD) camera equipped with 725 nm-short-pass and 532 nm-notch filters to avoid scattering from the incident probe and trapping beams. Figure 2, parts b and c, show images when a nanowire is optically trapped and oriented along the optical axis (Figure 2b) compared to when it is released from the trap (Figure 2c).

To study the second-order nonlinear responses from a free-standing nanowire, we first focused the trapping beam (532 nm CW, 200 mW) on a nanowire-dispersed aqueous solution through a high NA objective to trap a single nanowire. Only

dx.doi.org/10.1021/nl5011228 | Nano Lett. 2014, 14, 4322−4327

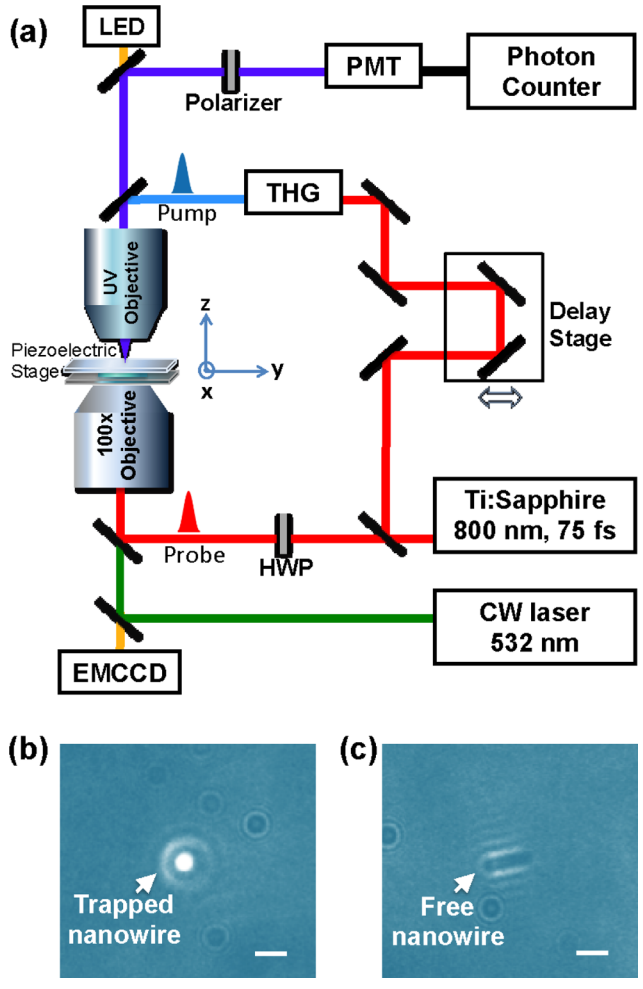

Figure 2. (a) Schematic diagram of the experimental setup. An 800 nm beam produces a pump beam via third harmonic generation (THG) and a probe beam. A 532 nm CW laser is used as a trapping beam. Optical images are collected using an EMCCD camera. SHG photons from nanowires are collected using a PMT detector and a photon counter. (b) EMCCD camera image (false color) of an optically trapped $KNbO_3$ nanowire in an aqueous solution. (c) EMCCD camera image (false color) of the nanowire when released from the trap. Scale bars, 2 μm.

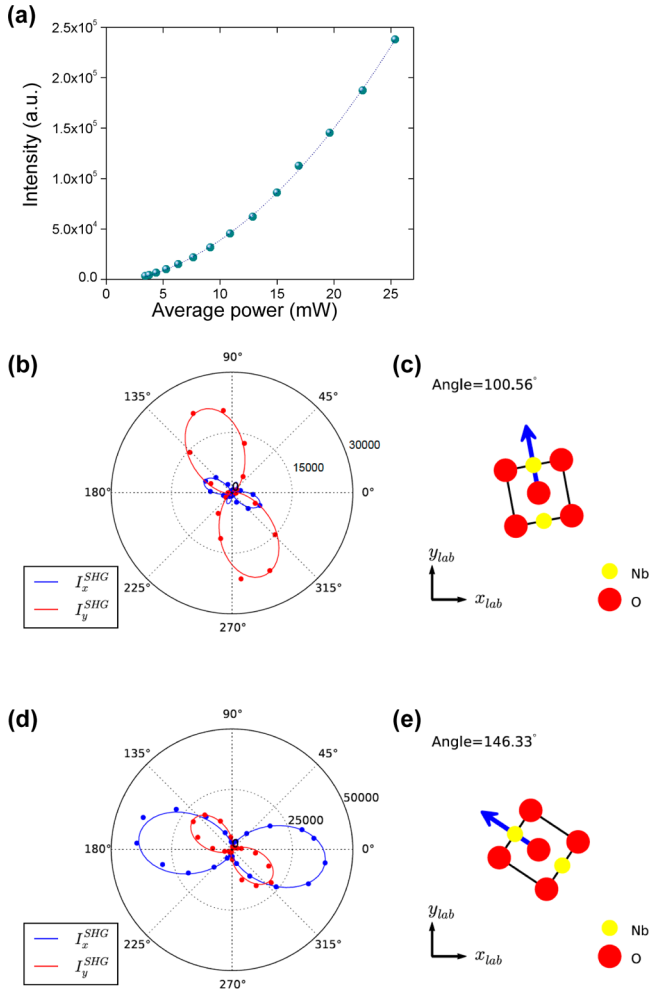

Figure 3. (a) SHG signals averaged from three optically trapped nanowires as a function of probe average power showing a quadratic response. (b) Polarization dependence of SHG observed from a trapped nanowire with a polarizer parallel to the *x*-axis (blue) and *y*-axis (red). (c) Schematic unit cell of the nanowire used in part b with an azimuthal angle of 100.56° for the spontaneous polarization direction (blue arrow). (d) Polar plots from another trapped nanowire. (e) Schematic unit cell of the nanowire used in part d with an azimuthal angle of 146.33° (blue arrow).

one nanowire was dragged into the trap at a time due to the tightly focused beam profile. We also found that relatively long nanowires were easy to trap because of the large drag coefficient.[37] When one nanowire is optically trapped, the long axis of the nanowire is oriented along the optical axis, leading to a 45° inclination of the spontaneous ferroelectric polarization to the optical axis, but with random azimuthal orientation with respect to the probe polarization. The incident probe beam generates SHG photons at 400 nm (just below the $KNbO_3$ optical bandgap) along the length of the nanowire, which are then collected through a UV objective (or a condenser) in a transmission geometry.[1]

Figure 3a shows the SHG signals measured from trapped nanowires as a function of probe average power. The quadratic responses from three different single nanowires were observed and averaged at different probe fluences from 0.08 to 0.6 J/cm^2. The expected quadratic response indicates that no significant perturbation of the nanowire is induced by the below-band gap probe excitation. To estimate achievable SHG photons from the standing nanowire, we calculated the SHG conversion efficiency[1,48] using a probe fluence of 0.1 J/cm^2. The measured SHG conversion efficiency from the standing nanowire is 2×10^{-3}, which is close to the calculated value of order 10^{-3} (See Supporting Information).

We examine the polarization dependence of the SHG signals from a trapped nanowire by rotating a half wave plate (HWP) in the incident probe beam. In parts b and d of Figure 3, we show SHG polar plots collected from two different trapped nanowires as a function of incident polarization angle. The SHG signals were measured with a polarizer output parallel to the *x*-axis (blue) and *y*-axis (red) defined in Figure 2. To understand the SHG polarization dependence, we calculate the SHG intensity at various incident polarizations based on a second-order nonlinear polarization model, accounting for the azimuthal dependence of the nanowire ferroelectric polarization axis with respect to the light polarization (Supporting Information).[1,48] The calculated SHG intensity (line) fits well to the experimentally measured SHG signals (dots) in both data. Parts c and e of Figure 3 show schematic models for the

dx.doi.org/10.1021/nl5011228 | *Nano Lett.* 2014, 14, 4322−4327

corresponding unit cells, calculated azimuthal angles of the nanowire with respect to the lab axes, and spontaneous polarization directions in the crystal lattice (blue arrow). Each trapped nanowire shows different polarization symmetries depending on various azimuthal orientations of the crystal lattice with respect to the lab axes, indicating that the nanowire is not spinning, consistent with prior reports.[49−51] One can therefore infer from the data the crystallographic azimuthal angle of the nanowire with respect to the trapping axis in the limit of a single nanostructure.

To investigate the response upon photoexcitation in a trapped nanowire, we measure femtosecond time-resolved SHG signals from the nanowire as a function of the pump−probe time delay, pumping with above-bandgap photons at 266 nm. Figure 4a shows the normalized SHG intensity collected

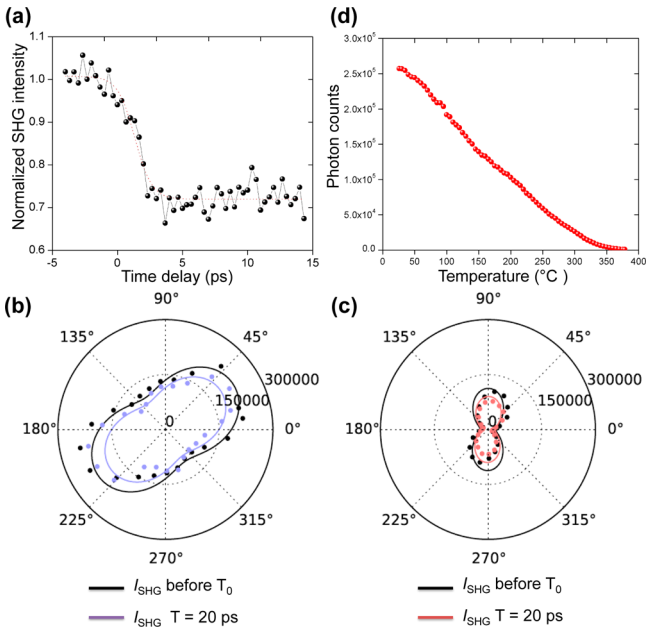

Figure 4. (a) Time-resolved SHG signals from a trapped nanowire as a function of pump−probe time delay upon photoexcitation (guideline in red dots). (b) SHG polar plots from a trapped nanowire before T_0 (black) and at t = 20 ps (purple) as a function of incident polarization angle measured with a polarizer parallel to the x-axis. (c) SHG polar plots from the nanowire before T_0 (black) and at t = 20 ps (red) as a function of incident polarization angle detected with a polarizer parallel to the y-axis. (d) Temperature-dependent SHG intensity measured from a nanowire powder upon heating up to T_c.

with 300 fs time steps, averaged over ten measurements. We observe a large amplitude (∼36%) photoinduced decrease in the SHG intensity occurring on a time-scale of 2−3 ps, indicating large amplitude changes in $\chi^{(2)}$, reversible at the 5 MHz repetition rate of the pump laser. Excitation conditions (assuming the absorption cross-section is determined by the nanowire diameter) correspond to approximately 10^{19} electron−hole pairs/nanowire which we estimate gives rise to negligible changes in the linear optical constants using a Drude model. This also implies that the reduced SHG intensity is not associated with changes in phase matching conditions upon photoexcitation. Parts b and c of Figure 4 show the corresponding optical polarization dependence comparing the result before time zero to the result obtained at t = 20 ps, with no significant change in the symmetry of the polarization plots observed. No evidence of recovery is observed in the first 20 ps after excitation. In the approximation that $\chi^{(2)}$ of the nanowire is linear in the ferroelectric polarization,[41,52,53] this corresponds to a modulation of the polarization of order 10% (with the SHG intensity varying quadratically with the polarization).[48] We note that photoinduced changes in $\chi^{(2)}$ in other materials have been attributed to carrier-induced modulations without associated structural modifications.[32,39,54] However, the 2−3 ps time scale observed here is inconsistent with an effect like this which would be expected to occur on instrument-limited time scales. Moreover, we also observe similar effects using pump and probe beams at 340 and 1030 nm, respectively, with 500 fs pulse width, indicating that the observed changes are not driven by nonthermal effects associated with nonequilibrium carrier densities but rather by the total energy absorbed by the nanowire (see Supporting Information). The few picosecond time-scales observed are consistent with electron−phonon coupling times measured in other perovskite ferroelectrics.[55]

In order to understand these large-amplitude photoinduced responses, we first carried out static temperature dependent measurements of the SHG intensity within a nanowire powder dried on a silicon wafer.[2] Figure 4d shows the result of heating up to the Curie temperature, T_c. At T_c, where the ferroelectric tetragonality and spontaneous polarization approach zero, the SHG intensity follows this trend as expected, with an observed T_c consistent with the X-ray measurements and known values in $KNbO_3$.[2] Evidence for the orthorhombic to tetragonal transition is observed as a slight change in slope of the temperature dependent measurements at the same temperature observed with X-ray probing, although this is broadened significantly. This temperature-dependent SHG data shows that a temperature jump of order 100 K is required to explain the above time-resolved measurements. In contrast, straightforward estimates of the induced temperature jump given known values for the bulk absorption coefficient[56] and specific heat[57] indicate induced temperature jumps of order 1 K averaged over the nanowire length. In this first approximation, the nanowire represents an effective cross-section determined by its diameter, and a 1 mJ/cm^2 incident fluence corresponds to an absorbed energy of ∼100 fJ. However, recent experiments have observed significantly enhanced nanowire effective cross sections for photoabsorption, with the nanowire acting like an antenna to concentrate the light field.[17,58] These effects have not been observed in ferroelectric nanowires previously, but the large dielectric constants of these materials make them prime candidates for effects such as this. In this picture, the nanowire, embedded within the light field of the pump pulse, experiences enhanced coupling to the electromagnetic field,[17] explaining the large amplitude effects observed. In order to investigate quantitatively this we have performed 3D finite difference time domain (FDTD) simulations using CST-Microwave Studio for a plane wave excitation at 266 nm to quantify the coupling of the applied pump pulse to the optically trapped nanowire (see Supporting Information), with input optical constants taken from bulk values.[56] Figure 5a shows the amplitude of the power flow (Poynting vector), showing that a significant amount of light couples into the nanowire sides, with an associated shadow observed along the boundaries of the nanowire reflecting the increased effective cross-section. The simulated directions of the power flow are shown in Figure 5b. Figure 5c shows the energy absorption per pulse within 1 nm transverse slices along the nanowire length, providing additional evidence for enhanced coupling of the light field into the nanowire with low internal optical loss along the nanowire.[59]

dx.doi.org/10.1021/nl5011228 | Nano Lett. 2014, 14, 4322−4327

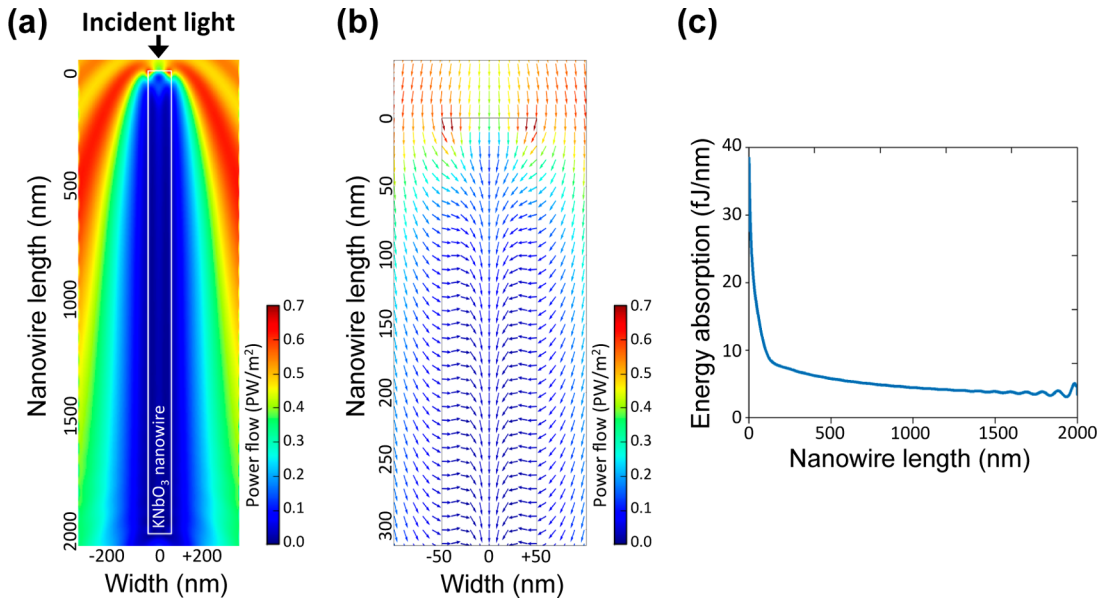

Figure 5. (a) FDTD simulation showing the amplitude of the power flow over a free-standing nanowire (white rectangular, 100 nm in diameter and 2 μm in length) in water. Incident plane wave (E = 0.53 GV/m, 50 fs) is propagating along the long axis of the nanowire. (b) Calculated directions of the power flow shown in part a. (c) Energy absorption distribution per pulse within successive 1 nm slices as a function of the nanowire length.

The calculated total energy absorbed is 3 pJ, corresponding to a temperature jump of 46 K averaged over the entire nanowire, with a 144 K temperature jump averaged over the first 100 nm of the nanowire. Although these calculations do not fully account for the coupling of the applied field to the ferroelectric polarization and the associated bound charge/depolarization field at the surface of the nanowire[11,13] or the crystallographic dependence of the optical constants, the calculated energy density deposited in the nanowire is sufficient to generate temperature jumps of the magnitude required to explain the anomalously large changes in $\chi^{(2)}$.

In summary, we present the first real-time femtosecond resolution nonlinear optical measurements of the dynamics of a single ferroelectric nanowire within an optical trap. Large amplitude photoinduced modulations in the nonlinear optical properties and polarization of single ferroelectric nanowires are observed, reversible at megahertz repetition rates. These are attributed to enhanced light absorption within the nanowire, with a diameter comparable to the optical wavelength. These effects indicate novel photoferroelectric coupling associated with ultrafast structural responses developing on a few picosecond time-scales, and open up new opportunities with respect to the development of light-driven nanoscale ferroelectric devices.

■ ASSOCIATED CONTENT

Supporting Information

Second harmonic generation conversion efficiency, model for polarization dependence of SHG, FDTD simulation, and time-resolved SHG responses using different excitation wavelengths. This material is available free of charge via the Internet at http://pubs.acs.org.

■ AUTHOR INFORMATION

Corresponding Author

*(A.M.L.) E-mail: aaronl@stanford.edu.

Author Contributions

⊥These authors contributed equally to this work.

S.N. and Y.K. carried out the pump−probe experiment and XRD measurements. F.C. and Y.K. carried out the FDTD simulations. J.P. and R.S. led the TEM characterization used within this work. A.M.L. initiated the project and conceived the work. S.N., Y.K., and A.M.L. wrote the manuscript with input from all authors.

Notes

The authors declare no competing financial interest.

■ ACKNOWLEDGMENTS

Research supported by the National Science Foundation (NSF) under Grant No. 1310545 (laser experiments) and the U.S. Department of Energy (DOE), Office of Science, Basic Energy Sciences (BES), under Contract Number DE-AC02-76-SFO0515 (XRD, sample synthesis, FDTD simulations). F.C. acknowledges support in part by a NSF Graduate Research Fellowship. J.P. was supported by the Center on Nanostructuring for Efficient Energy Conversion (CNEEC), an Energy Frontier Research Center funded by the US Department of Energy, Office of Science, Office of Basic Energy Sciences, under Award Number DE-SC0001060.

■ REFERENCES

(1) Nakayama, Y.; Pauzauskie, P. J.; Radenovic, A.; Onorato, R. M.; Saykally, R. J.; Liphardt, J.; Yang, P. *Nature* **2007**, *447* (7148), 1098−1101.

(2) Gopalan, V.; Raj, R. *Appl. Phys. Lett.* **1996**, *68* (10), 1323−1325.

(3) Liang, L. Y.; Li, Y. L.; Chen, L. Q.; Hu, S. Y.; Lu, G. H. *J. Appl. Phys.* **2009**, *106* (10), 104118.

(4) Zysset, B.; Biaggio, I.; Gunter, P. *J. Opt. Soc. Am. B* **1992**, *9* (3), 380−386.

(5) Yang, Y.; Jung, J. H.; Yun, B. K.; Zhang, F.; Pradel, K. C.; Guo, W.; Wang, Z. L. *Adv. Mater.* **2012**, *24* (39), 5357−5362.

(6) Saito, Y.; Takao, H.; Tani, T.; Nonoyama, T.; Takatori, K.; Homma, T.; Nagaya, T.; Nakamura, M. *Nature* **2004**, *432* (7013), 84−87.

(7) Lummen, T. T.; Gu, Y.; Wang, J.; Lei, S.; Xue, F.; Kumar, A.; Barnes, A. T.; Barnes, E.; Denev, S.; Belianinov, A.; Holt, M.;

Morozovska, A. N.; Kalinin, S. V.; Chen, L. Q.; Gopalan, V. *Nat. Commun.* **2014**, *5*, 3172.
(8) Louis, L.; Gemeiner, P.; Ponomareva, I.; Bellaiche, L.; Geneste, G.; Ma, W.; Setter, N.; Dkhil, B. *Nano Lett.* **2010**, *10* (4), 1177−1183.
(9) Kim, S.; Lee, J. H.; Lee, J.; Kim, S. W.; Kim, M. H.; Park, S.; Chung, H.; Kim, Y. I.; Kim, W. *J. Am. Chem. Soc.* **2013**, *135* (1), 6−9.
(10) Kreisel, J.; Alexe, M.; Thomas, P. A. *Nat. Mater.* **2012**, *11* (4), 260.
(11) Daranciang, D.; Highland, M. J.; Wen, H.; Young, S. M.; Brandt, N. C.; Hwang, H. Y.; Vattilana, M.; Nicoul, M.; Quirin, F.; Goodfellow, J.; Qi, T.; Grinberg, I.; Fritz, D. M.; Cammarata, M.; Zhu, D.; Lemke, H. T.; Walko, D. A.; Dufresne, E. M.; Li, Y.; Larsson, J.; Reis, D. A.; Sokolowski-Tinten, K.; Nelson, K. A.; Rappe, A. M.; Fuoss, P. H.; Stephenson, G. B.; Lindenberg, A. M. *Phys. Rev. Lett.* **2012**, *108* (8), 087601.
(12) Kundys, B.; Viret, M.; Colson, D.; Kundys, D. O. *Nat. Mater.* **2010**, *9* (10), 803−805.
(13) Schick, D.; Herzog, M.; Wen, H.; Chen, P.; Adamo, C.; Gaal, P.; Schlom, D. G.; Evans, P. G.; Li, Y.; Bargheer, M. *Phys. Rev. Lett.* **2014**, *112* (9), 097602.
(14) Ponomareva, I.; Bellaiche, L. *Phys. Rev. Lett.* **2008**, *101* (19), 197602.
(15) Schmising, C. v. K.; Bargheer, M.; Kiel, M.; Zhavoronkov, N.; Woerner, M.; Elsaesser, T.; Vrejoiu, I.; Hesse, D.; Alexe, M. *Phys. Rev. Lett.* **2007**, *98* (25), 257601.
(16) Dougherty, T. P.; Wiederrecht, G. P.; Nelson, K. A.; Garrett, M. H.; Jensen, H. P.; Warde, C. *Science* **1992**, *258* (5083), 770−774.
(17) Krogstrup, P.; Jorgensen, H. I.; Heiss, M.; Demichel, O.; Holm, J. V.; Aagesen, M.; Nygard, J.; Morral, A. F. I. *Nat. Photonics* **2013**, *7* (4), 306−310.
(18) Sirbuly, D. J.; Law, M.; Pauzauskie, P.; Yan, H.; Maslov, A. V.; Knutsen, K.; Ning, C. Z.; Saykally, R. J.; Yang, P. *Proc. Natl. Acad. Sci. U.S.A.* **2005**, *102* (22), 7800−7805.
(19) Jung, J. H.; Lee, M.; Hong, J. I.; Ding, Y.; Chen, C. Y.; Chou, L. J.; Wang, Z. L. *ACS Nano* **2011**, *5* (12), 10041−10046.
(20) Schlom, D. G.; Chen, L.-Q.; Fennie, C. J.; Gopalan, V.; Muller, D. A.; Pan, X.; Ramesh, R.; Uecker, R. *MRS Bull.* **2014**, *39* (02), 118−130.
(21) Fu, H.; Cohen, R. E. *Nature* **2000**, *403* (6767), 281−283.
(22) Shirane, G.; Newnham, R.; Pepinsky, R. *Phys. Rev.* **1954**, *96* (3), 581−588.
(23) Wang, J.; Stampfer, C.; Roman, C.; Ma, W. H.; Setter, N.; Hierold, C. *Appl. Phys. Lett.* **2008**, *93* (22), 223101.
(24) Suyal, G.; Colla, E.; Gysel, R.; Cantoni, M.; Setter, N. *Nano Lett.* **2004**, *4* (7), 1339−1342.
(25) Zheng, H.; Rivest, J. B.; Miller, T. A.; Sadtler, B.; Lindenberg, A.; Toney, M. F.; Wang, L. W.; Kisielowski, C.; Alivisatos, A. P. *Science* **2011**, *333* (6039), 206−209.
(26) Miller, T. A.; Wittenberg, J. S.; Wen, H.; Connor, S.; Cui, Y.; Lindenberg, A. M. *Nat. Commun.* **2013**, *4*, 1369.
(27) Clark, J. N.; Beitra, L.; Xiong, G.; Higginbotham, A.; Fritz, D. M.; Lemke, H. T.; Zhu, D.; Chollet, M.; Williams, G. J.; Messerschmidt, M.; Abbey, B.; Harder, R. J.; Korsunsky, A. M.; Wark, J. S.; Robinson, I. K. *Science* **2013**, *341* (6141), 56−59.
(28) van der Veen, R. M.; Kwon, O. H.; Tissot, A.; Hauser, A.; Zewail, A. H. *Nat. Chem.* **2013**, *5* (5), 395−402.
(29) Gao, B.; Hartland, G. V.; Huang, L. *ACS Nano* **2012**, *6* (6), 5083−5090.
(30) Mehl, B. P.; Kirschbrown, J. R.; House, R. L.; Papanikolas, J. M. *J. Phys. Chem. Lett.* **2011**, *2* (14), 1777−1781.
(31) Hartland, G. V. *Chem. Sci.* **2010**, *1* (3), 303−309.
(32) Johnson, J. C.; Knutsen, K. P.; Yan, H. Q.; Law, M.; Zhang, Y. F.; Yang, P. D.; Saykally, R. J. *Nano Lett.* **2004**, *4* (2), 197−204.
(33) Ruijgrok, P. V.; Zijlstra, P.; Tchebotareva, A. L.; Orrit, M. *Nano Lett.* **2012**, *12* (2), 1063−1069.
(34) Pauzauskie, P. J.; Radenovic, A.; Trepagnier, E.; Shroff, H.; Yang, P. D.; Liphardt, J. *Nat. Mater.* **2006**, *5* (2), 97−101.
(35) Marago, O. M.; Jones, P. H.; Gucciardi, P. G.; Volpe, G.; Ferrari, A. C. *Nat. Nanotechnol.* **2013**, *8* (11), 807−819.
(36) Dutto, F.; Raillon, C.; Schenk, K.; Radenovic, A. *Nano Lett.* **2011**, *11* (6), 2517−2521.
(37) Reece, P. J.; Toe, W. J.; Wang, F.; Paiman, S.; Gao, Q.; Tan, H. H.; Jagadish, C. *Nano Lett.* **2011**, *11* (6), 2375−2381.
(38) Wang, F.; Toe, W. J.; Lee, W. M.; McGloin, D.; Gao, Q.; Tan, H. H.; Jagadish, C.; Reece, P. J. *Nano Lett.* **2013**, *13* (3), 1185−1191.
(39) Schaller, R. D.; Johnson, J. C.; Saykally, R. J. *ChemPhysChem* **2003**, *4* (11), 1243−1247.
(40) Neacsu, C. C.; van Aken, B. B.; Fiebig, M.; Raschke, M. B. *Phys. Rev. B* **2009**, *79* (10), 100107.
(41) Murgan, R.; Tilley, D. R.; Ishibashi, Y.; Webb, J. F.; Osman, J. *J. Opt. Soc. Am. B* **2002**, *19* (9), 2007−2021.
(42) Denev, S. A.; Lummen, T. T. A.; Barnes, E.; Kumar, A.; Gopalan, V. *J. Am. Ceram. Soc.* **2011**, *94* (9), 2699−2727.
(43) Lisha, Y.; Jun, Z.; Xuemei, Z.; Xiaoxing, W.; Jinyao, L.; Yinshu, W.; Gang, L.; Jiaguo, Y.; Linjie, Z. *Int. J. Hydrogen Energy* **2013**, *38* (9), 3554−3561.
(44) Gopalan, V.; Raj, R. *J. Am. Ceram. Soc.* **1995**, *78* (7), 1825−1833.
(45) Murzina, T. V.; Savinov, S. A.; Ezhov, A. A.; Aktsipetrov, O. A.; Korsakov, I. E.; Bolshakov, I. A.; Kaul, A. R. *Appl. Phys. Lett.* **2006**, *89* (6), 062907.
(46) Wang, G.; Selbach, S. M.; Yu, Y.; Zhang, X.; Grande, T.; Einarsrud, M.-A. *CrystEngComm* **2009**, *11* (9), 1958−1963.
(47) Magrez, A.; Vasco, E.; Seo, J. W.; Dieker, C.; Setter, N.; Forro, L. *J. Phys. Chem. B* **2006**, *110* (1), 58−61.
(48) Gopalan, V.; Raj, R. *J. Am. Ceram. Soc.* **1996**, *79* (12), 3289−3296.
(49) Friese, M. E. J.; Nieminen, T. A.; Heckenberg, N. R.; Rubinsztein-Dunlop, H. *Nature* **1998**, *394*, 348−350.
(50) Xu, X.; Cheng, C.; Xin, H.; Lei, H.; Li, B. *Sci. Rep.* **2014**, *4*, 3989.
(51) Tong, L.; Miljković, V. D.; Käll, M. *Nano Lett.* **2010**, *10*, 268−273.
(52) Mishina, E. D.; Sherstyuk, N. E.; Stadnichuk, V. I.; Sigov, A. S.; Mukhorotov, V. M.; Golovko, Y. I.; van Etteger, A.; Rasing, T. *Appl. Phys. Lett.* **2003**, *83* (12), 2402−2404.
(53) Liu, S. W.; Chakhalian, J.; Xiao, M.; Chen, C. L. *Appl. Phys. Lett.* **2007**, *90* (4), 042901.
(54) Son, D. H.; Wittenberg, J. S.; Banin, U.; Alivisatos, A. P. *J. Phys. Chem. B* **2006**, *110* (40), 19884−19890.
(55) Acharya, S.; Chouthe, S.; Graener, H.; Böntgen, T.; Sturm, C.; Schmidt-Grund, R.; Grundmann, M.; Seifert, G. *J. Appl. Phys.* **2014**, *115* (5), 053508.
(56) Palik, E. D. *Handbook of Optical Constants of Solids*; Academic Press: New York, 1985; p 804.
(57) Busse, L. E.; Goldberg, L.; Surette, M. R.; Mizell, G. *J. Appl. Phys.* **1994**, *75* (2), 1102−1110.
(58) Wallentin, J.; Anttu, N.; Asoli, D.; Huffman, M.; Aberg, I.; Magnusson, M. H.; Siefer, G.; Fuss-Kailuweit, P.; Dimroth, F.; Witzigmann, B.; Xu, H. Q.; Samuelson, L.; Deppert, K.; Borgstrom, M. T. *Science* **2013**, *339* (6123), 1057−1060.
(59) Brongersma, M. L.; Cui, Y.; Fan, S. *Nat. Mater.* **2014**, *13*, 451−460.